ACS OMEGA

http://pubs.acs.org/journal/acsodf

Article

One-Pot Biosynthesis of Carbon-Coated Silver Nanoparticles Using Palm Leaves as a Reductant and a Carbon Source

Xuchao Jian,[§] Ying Wang,[§] Rukang Zhu, Yingying Pan, Huangqing Ye,* and Xiping Zeng*

Cite This: *ACS Omega* 2023, 8, 23607−23612

Read Online

ACCESS | Metrics & More | Article Recommendations | Supporting Information

ABSTRACT: In this study, carbon-coated silver nanoparticles (Ag@C NPs) were synthesized with a one-pot hydrothermal method using palm leaves as a reductant and a carbon source. SEM, TEM, XRD, Raman, and UV−vis analyses were employed to characterize the as-prepared Ag@C NPs. Results showed that the diameter of silver nanoparticles (Ag NPs) and the coating thickness could be controlled by changing the amount of biomass and the reaction temperature. The diameter ranged from 68.33 to 143.15 nm, while the coating thickness ranged from 1.74 to 4.70 nm. As the biomass amount and the reaction temperature increased, the diameter of Ag NPs and the coating thickness became larger. Thus, this work provided a green, simple, and feasible method for the preparation of metal nanocrystals.

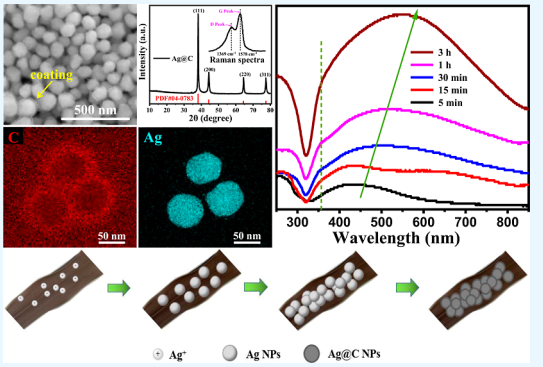

1. INTRODUCTION

Noble metal nanoparticles, particularly Ag NPs, are being favored by researchers because of their wide application in various fields,[1] such as antibacterial,[2] sensing,[3] nanomedicine,[4] electronics,[5,6] and so on. These applications of Ag NPs are attributed to their unique chemical and physical properties, which are strongly influenced by their size, distribution, morphology, shape, and surface characteristics.[7] Therefore, the investigation of the synthesis method of Ag NPs is the key to achieving its controllable preparation and mass production.[8,9] At present, the common methods cover physical and chemical methods.[8,10] Physical methods include magnetron sputtering,[11] vacuum condensation,[12] laser ablation,[13] and so on, which are commonly expensive. Meanwhile, chemical methods include the electrochemical method,[14] wet chemical method,[15] microwave-assisted method,[16] and so on, in which the equipment process is inexpensive but harmful to the environment.[17] Hence, increasing numbers of researchers have begun to develop low-cost and green reductants. For example, L-cysteine was used to synthesize supramolecular hydrogel-containing amino acid-stabilized silver nanoparticles.[18] A simple and facile synthesis route to prepare gold and silver nanoparticles on bacterial cellulose nanofiber films was also proposed.[19] Lately, Yao reported on the development of a mild synthesis method for the facile fabrication of silver nanoparticles within a confined microenvironment created by dendronized chitosan oligosaccharides.[20] Moreover, a novel approach using plant embryos for green synthesis of silver nanoparticles was reported.[21]

As is known, silver migration is a key factor that affects the application of Ag NPs.[6] The common solution is to coat Ag NPs with some substances, such as glutathione,[22] carbonates,[23] silica,[24] and so on. Generally, the structural characteristics of these coatings greatly influence the properties of Ag NPs, and an increasing number of researchers prefer to use conductive materials as coatings because of their relatively little effect on the conductivity of silver.

Herein, the present study proposes a simple, low-cost, and stable one-pot synthesis of Ag@C NPs using biomass as a reductant and a carbon source. In addition, the effects of biomass amount and reaction temperature on the particle size and coating thickness of the as-prepared products have been discussed comprehensively while the possible growth mechanism of carbon-coated silver is presented. This one-pot hydrothermal method is simple, cheap, green, and scalable. Moreover, the kind of as-prepared special-structured Ag NPs biosynthesized with palm leaves might have great potential application in various areas.

2. EXPERIMENTAL SECTION

2.1. Raw Materials. Silver nitrate ($AgNO_3$, ≥99.0%, AR, Sinopharm Group Chemical Reagent Co., Ltd., China) and ethanol (C_2H_5OH, 99.7%, Sinopharm Chemical Reagent Co., Ltd., China) were used in this study. The palm leaves were obtained in Shenzhen, Guangdong Province, China. All

Received: March 7, 2023
Accepted: May 3, 2023
Published: June 23, 2023

chemical reagents were used without further purification or treatment. Deionized Mini-Q water produced in the lab (specific resistance above 18.0 MΩ cm) was used throughout the experiments.

2.2. Preparation of Ag NPs. The palm leaves (Figure S1) were cut into ∼3 cm squares and cleaned using deionized water to remove surface dust and then dried at 60 °C for a week to dehydrate them completely. For experimental stability, the middle part of the dried leaves was used. First, 0.05 g of $AgNO_3$ was dissolved in 40 mL of deionized water under ultrasonic conditions. Then, 0.03 g of dry palm leaf chunks were directly added to the $AgNO_3$ solution above. Finally, the mixture was carefully transferred into a 50 mL Teflon-lined autoclave and heated at 150 °C for 3 h. The precipitate was washed with water and ethanol and preserved in the ethanol solution.

2.3. Characterization. The as-prepared Ag@C NPs were oven-dried at 60 °C, and the powder was used for the following characterization. Then, the elemental composition and structure of the product were obtained using Raman spectroscopy (Raman, Horiba LabRam HR-800) and X-ray diffraction (XRD, Rigaku D/Max 2500, Japan). Surface morphologies were obtained by field-emission scanning electron microscopy (SEM, Hitachi Regulus 8100) and high-resolution transmission electron microscopy (HRTEM, FEI Talos F200X G2). In addition, a UV−visible spectrometer (UV−Vis, Shimadzu, UV-2600i, Japan) was used to characterize the diluted reaction solution of the as-prepared products. Thermogravimetric analysis (TGA) was conducted on a TA Instruments Q600 analyzer with a heating rate of 10 °C min^{-1}.

3. RESULTS AND DISCUSSION

Figure 1 shows the schematic diagram of the synthesis procedure of Ag@C NPs. The reactants were only water,

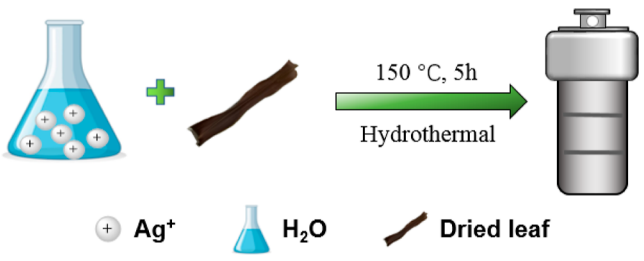

Figure 1. Schematic diagram of the synthesis procedure.

silver nitrate, and dried palm leaves, and the reaction condition was a one-pot hydrothermal method, which illustrates that the experimental method was simple and green.

Therefore, for the effects of different reduction doses on the morphology of products to be investigated, we, respectively, selected six different leaf dosage reactions for comparison, which were 10, 20, 30, 40, 50, and 100 mg. As shown in Figure S2, the products obtained from the six reactions were all Ag@C NPs. Thus, with the increase in blade dosage; the coating layer became increasingly evident and the thickness of the coating layer increased. We hypothesized that when the biomass amount was small, the number of organic molecules in the reaction system was also tiny; thus, the coating layer of the as-prepared products was thin. Furthermore, as the biomass and the amount of small organic molecules increased, the coating layer became thicker.

Then, the morphologies of Ag@C NPs prepared at different reaction temperatures were studied, as shown in Figure 2. The morphologies of the as-prepared products were very different at 120, 150, 180, and 200 °C. The diameter size distribution and average diameter of approximately 100 Ag NPs were calculated at each temperature. Results showed that the average diameter of the Ag NPs increased with the increase in temperature. This phenomenon was primarily caused by a hydrothermal process in which leaves were used as reductants, which was a kinetics-controlled process. As the temperature increased, the speed of reductant release on leaves became faster, and the amount of reductant consequently increased. Meanwhile, as the temperature increased and the reduction rate accelerated, the diameter of the as-prepared products became larger.

Moreover, temperature had an important effect on hydrothermal carbonization. Figure S3 shows the SEM−EDS analysis of the products prepared at four temperatures. The carbon content of the products gradually increased with the increase in temperature. This was because hydrolysis reactions occurred in leaves at low temperatures, and the contribution of the hydrothermal carbonization reaction increased with the temperature increasing. As the signal from SEM−EDS mainly originated on the sample surface, TGA was introduced to determine a more accurate carbon content in each product, shown in Figure S4. The weight change for pure silver during TGA should be 100%, so we can roughly get the silver content in the product, along with the carbon content. Similar to our previous results,[25] it is much lower than that found via SEM−EDS (Figure S4), which could be caused by the fact that the carbon element is mainly on the surface of the as-prepared product.

Subsequently, HRTEM was used to characterize their microstructure. Figure 3 shows the HRTEM image of the sample after the reaction at 150 °C for 5 h, from which we saw that the as-prepared products had evident coating structures. The typical area was selected for amplification observation (Figure 3c), and the lattice spacing was approximately 0.236 nm, which exactly corresponded to the XRD diffraction peak, thereby indicating that the silver elemental was successfully synthesized. By further energy spectrum analysis, we found that the as-prepared products at 150 °C for 5 h was primarily composed of C and Ag, and carbon was mainly concentrated on the surface of the particles. We preliminarily speculated that the as-prepared products were carbon-coated Ag NPs. Figures S5−S7 shows the HAADF-STEM and element distribution of the reaction products at 120, 180, and 200 °C, respectively. The thickness of the carbon coating increased with the increase in temperature, ranging from 1.74 to 4.70 nm as compared with the TEM magnification. By comparing the element distribution image, we knew that the carbon coating layer became more obvious with the increase in temperature, which was consistent with the literature.[25]

Herein, we used XRD and Raman to characterize the samples in Figure 4 to further verify the structural characteristics of the carbon coating. As shown in Figure 4a, the as-prepared products had four strong peaks at 2θ values of 38.116, 44.277, 64.426, and 77.472, corresponding to (111), (200), (220), and (311) of the face-centered cubic structure of silver, respectively, which were matched with JCPDF#04-0783. In Figure 4b, D- and G-band signal peaks of carbon appearing in Raman spectra also indicated that the particle had carbon

https://doi.org/10.1021/acsomega.3c01554
ACS Omega 2023, 8, 23607−23612

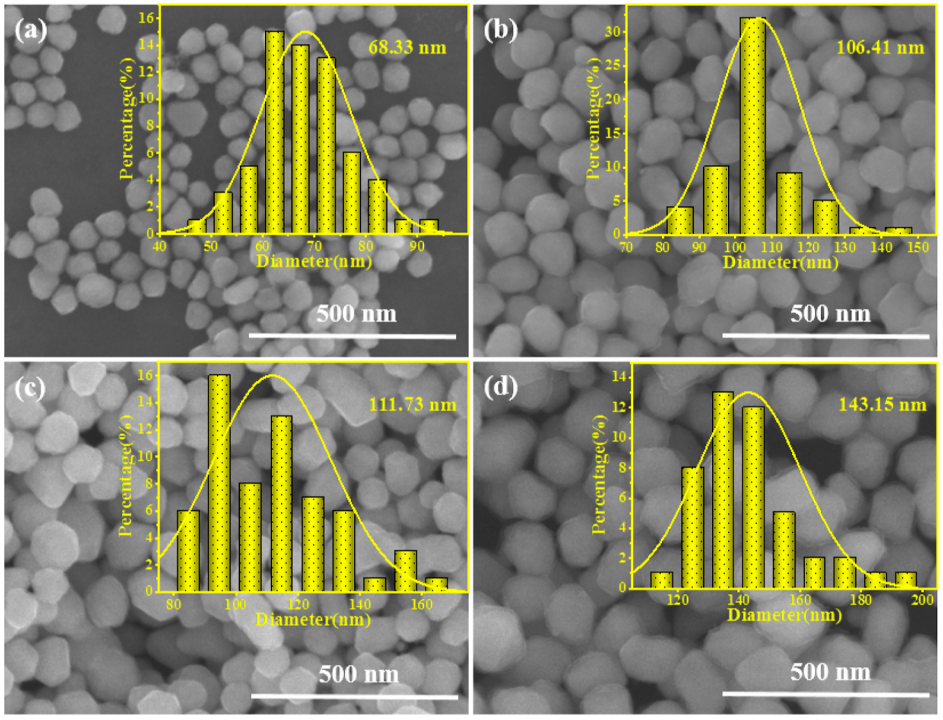

Figure 2. Elemental analysis by SEM−EDS of the as-prepared products at various reaction temperatures: (a) 120; (b) 150; (c) 180; and (d) 200 °C.

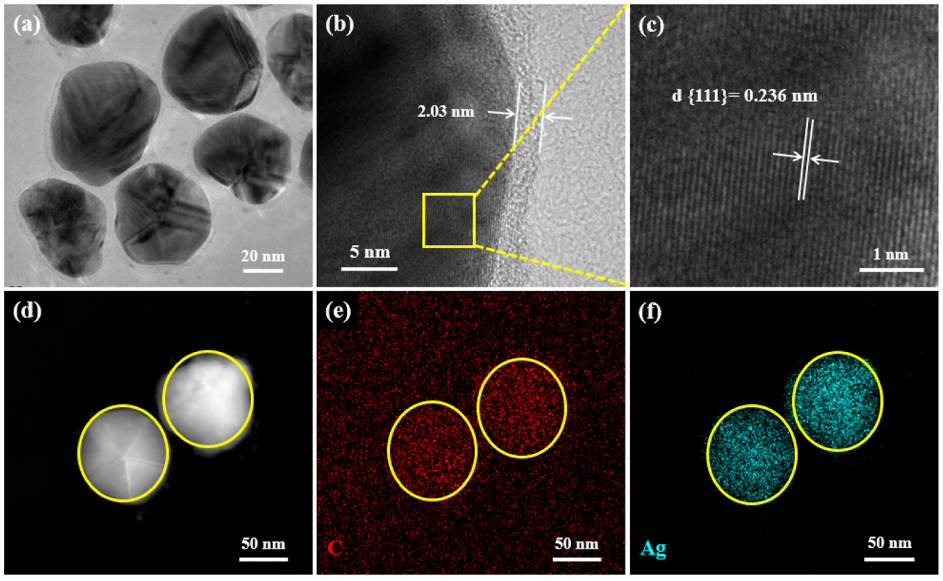

Figure 3. (a−c) HRTEM images and (d−f) HAADF-STEM elemental mapping images of the as-prepared products at 150 °C for 5 h.

composition, that is carbon-coated silver nanoparticles (Ag@C NPs).[26]

Therefore, SEM was introduced to characterize the samples at the reaction time of 0 min−3 h to analyze the whole growth mechanism of the Ag@C NPs. As shown in Figure 5a,b, the surface of the blade was smooth at the beginning, and after 5 min, various Ag NPs started to appear. Then, the number and diameter of the Ag NPs increased, and the coating layer on the surface of the Ag NPs gradually became increasingly clearer from 15 min onward. Furthermore, we used UV−vis spectra to characterize these samples. As shown in Figure S8, the absorbance maximum from Ag NPs increased in amplitude with the reaction time and showed a red shift, thereby indicating that the number and the size of the Ag NPs increased over time, which was consistent with the SEM results. Moreover, there was an absorbance peak at about 350 nm, which might be a signal of carbon-related substances.

The growth mechanism of Ag@C NPs is described in Figure 6 based on the above discussion. At the initial stage, the leaf hydrolyzed under the action of water and heat, thereby slowly releasing small organic molecules, like furfural, hydroxymethylfurfural, glucose, maltose, fructose, sucrose, and some acids.[25,27,28] At this time, with these molecules serving as reducing and capping agents, the silver ions adsorbed on the

https://doi.org/10.1021/acsomega.3c01554
ACS Omega 2023, 8, 23607−23612

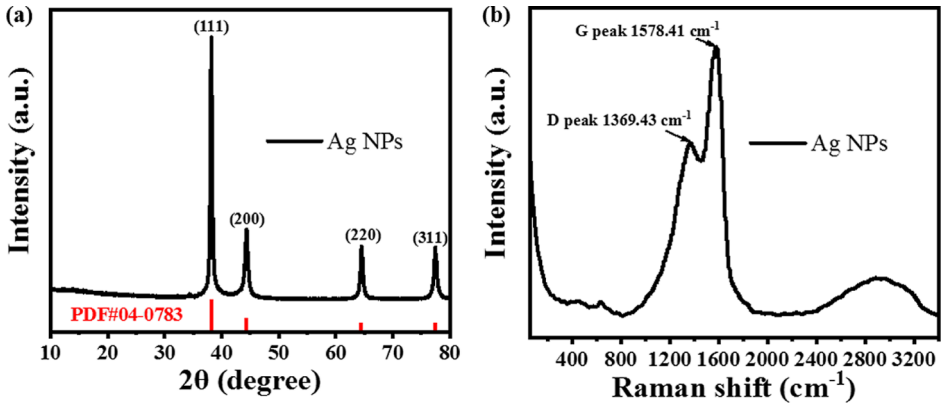

Figure 4. (a) XRD curves and (b) Raman curves of the as-prepared products at 150 °C for 5 h.

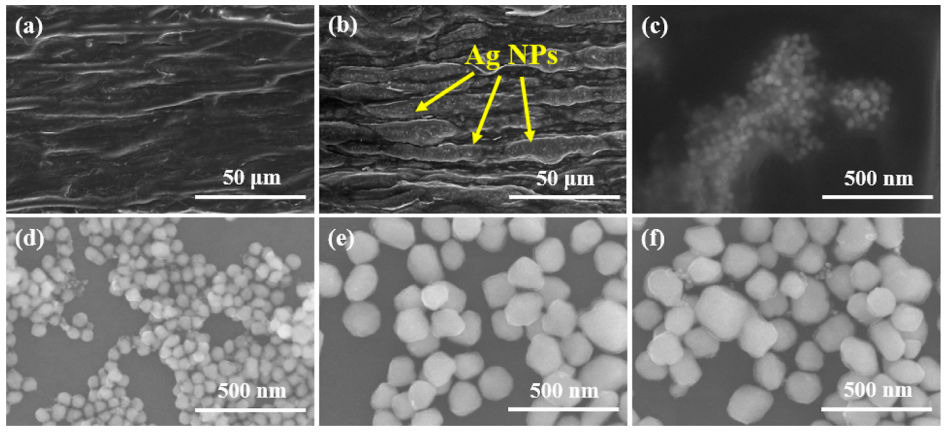

Figure 5. SEM images of the as-prepared products at 150 °C for various reaction times: (a) 0 min; (b) 5 min; (c) 15 min; (d) 30 min; (e) 1 h; and (f) 3 h.

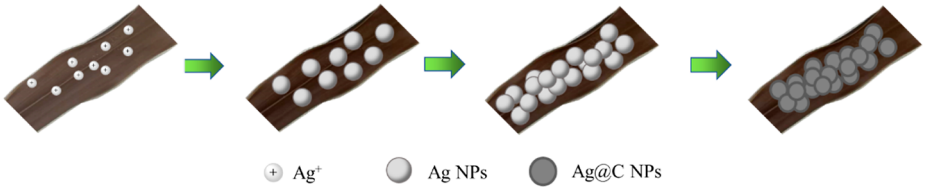

Figure 6. Schematic diagram of the growth mechanism of Ag@C NPs.

leaf surface were reduced to Ag NPs. Then, an increasing number of Ag NPs was formed over time, and their diameters also significantly increased. When most silver ions were reduced, the carbonization reaction[28,29] via further intermolecular dehydration began to play a dominant role as compared to the hydrolysis reaction. Eventually, the prepared Ag NPs were carbon-coated.

Finally, a certain amplification experiment was carried out in preparing the Ag@C NPs. The morphologies of the products of different volume amplification reactions are shown in Figure S9, which were similar to the products obtained by the reaction volume of 50 mL. The products prepared by the amplification reaction were also uniformly sized Ag@C NPs. The results above indicated that the reaction was scalable for mass production.

4. CONCLUSIONS

Ag@C NPs were successfully synthesized using biomass as a reducing agent and carbon source. This one-pot hydrothermal method was simple, cheap, green, and scalable. At the same time, with the increase of the biomass amount and reaction temperature, the diameter of the synthesized Ag NPs and the coating thickness became larger. This special structured Ag@C NPs biosynthesized with palm leaves might have great potential application in various areas.

SUPPORTING INFORMATION

Digital images of fresh leaf of Palm tree used for the synthesis; SEM images of the as-prepared products at 150 °C for various amount of leaves; HAADF-STEM elemental mapping images of the as-prepared products at various reaction temperatures; TGA results and histogram of carbon content determined by SEM−EDS and TGA of the as-prepared products; HRTEM and HAADF-STEM elemental mapping images of the as-prepared products at 120 °C, 180 °C, and 200 °C for 5 h; UV−vis spectra of the as-prepared products at 150 °C for various reaction times; and SEM images of the as-

https://doi.org/10.1021/acsomega.3c01554
ACS Omega 2023, 8, 23607−23612

prepared products for the scale-up reaction at different volumes (PDF)

■ ASSOCIATED CONTENT

Supporting Information

The Supporting Information is available free of charge at https://pubs.acs.org/doi/10.1021/acsomega.3c01554.

(PDF)

■ AUTHOR INFORMATION

Corresponding Authors

Huangqing Ye − *International Collaborative Laboratory of 2D Materials for Optoelectronics Science and Technology of Ministry of Education, Institute of Microscale Optoelectronics, Shenzhen University, Shenzhen 518060, China;* orcid.org/0000-0002-2324-5604; Email: beyondye88@gmail.com

Xiping Zeng − *Research and Develop Center, Shenzhen Huake-Tek Co., Ltd., Shenzhen 518116, China;* orcid.org/0000-0003-4002-347X; Email: xzengad@connect.ust.hk

Authors

Xuchao Jian − *Research and Develop Center, Shenzhen Huake-Tek Co., Ltd., Shenzhen 518116, China*

Ying Wang − *Research and Develop Center, Shenzhen Huake-Tek Co., Ltd., Shenzhen 518116, China*

Rukang Zhu − *Research and Develop Center, Shenzhen Huake-Tek Co., Ltd., Shenzhen 518116, China*

Yingying Pan − *Research and Develop Center, Shenzhen Huake-Tek Co., Ltd., Shenzhen 518116, China*

Complete contact information is available at: https://pubs.acs.org/10.1021/acsomega.3c01554

Author Contributions

[§]X.J. and Y.W. contributed equally to this work.

Notes

The authors declare no competing financial interest.

■ ACKNOWLEDGMENTS

This work was supported by the Natural Science Foundation of China (Grant nos. 61705137 and 52002250), the Science and Technology Project of Shenzhen (no. KQJSCX20180328093614762), and the Shenzhen Peacock Plan (no. KQTD2016022614361432). The authors acknowledge the assistance of the Instrumental Analysis Center of Shenzhen University (Lihu Campus) for XRD and UV−vis analysis. The authors would like to acknowledge the characterization assistance of Shiyanjia Lab (www.shiyanjia.com).

■ REFERENCES

(1) (a) Gao, C.; Lyu, F.; Yin, Y. Encapsulated Metal Nanoparticles for Catalysis. *Chem. Rev.* **2021**, *121*, 834−881. (b) Nilghaz, A.; Mousavi, S. M.; Tian, J.; Cao, R.; Guijt, R. M.; Wang, X. Noble-Metal Nanoparticle-Based Colorimetric Diagnostic Assays for Point-of-Need Applications. *ACS Appl. Nano Mater.* **2021**, *4*, 12808−12824.

(2) McNamara, K.; Tofail, S. A. M. Nanoparticles in biomedical applications. *Adv. Phys.: X* **2017**, *2*, 54−88.

(3) Shen, L.; Chen, M.; Hu, L.; Chen, X.; Wang, J. Growth and Stabilization of Silver Nanoparticles on Carbon Dots and Sensing Application. *Langmuir* **2013**, *29*, 16135−16140.

(4) Lee, S. H.; Jun, B.-H. Silver Nanoparticles: Synthesis and Application for Nanomedicine. *Int. J. Mol. Sci.* **2019**, *20*, 865.

(5) Qi, L.; Lee, B. I.; Chen, S.; Samuels, W. D.; Exarhos, G. J. High-Dielectric-Constant Silver−Epoxy Composites as Embedded Dielectrics. *Adv. Mater.* **2005**, *17*, 1777−1781 (accessed Feb 24, 2023).

(6) Li, Y.; Wong, C. P. Monolayer protection for migration control in silver nanocomposite. *Appl. Phys. Lett.* **2006**, *89*, 112112.

(7) Alivisatos, A. P. Perspectives on the Physical Chemistry of Semiconductor Nanocrystals. *J. Phys. Chem.* **1996**, *100*, 13226−13239.

(8) Xie, J.; Lee, J. Y.; Wang, D. I. C.; Ting, Y. P. Silver Nanoplates: From Biological to Biomimetic Synthesis. *ACS Nano* **2007**, *1*, 429−439.

(9) (a) Narayanan, K. B.; Sakthivel, N. Biological synthesis of metal nanoparticles by microbes. *Adv. Colloid Interface Sci.* **2010**, *156*, 1−13. (b) Pestov, A.; Nazirov, A.; Modin, E.; Mironenko, A.; Bratskaya, S. Mechanism of Au(III) reduction by chitosan: Comprehensive study with 13C and 1H NMR analysis of chitosan degradation products. *Carbohydr. Polym.* **2015**, *117*, 70−77. (c) Raveendran, P.; Fu, J.; Wallen, S. L. Completely "Green" Synthesis and Stabilization of Metal Nanoparticles. *J. Am. Chem. Soc.* **2003**, *125*, 13940−13941. (d) Ye, H.; Zhuang, G.; Pan, Y.; Wang, H.; Li, Y.; Lin, Y.; Wang, Y.; Zeng, X. Controllable synthesis of silver nanowires via an organic cation-mediated polyol method and their application as transparent electrode for touch screen. *Nano Select* **2022**, *3*, 1306−1313.

(10) (a) Chen, D.; Qiao, X.; Qiu, X.; Chen, J. Synthesis and electrical properties of uniform silver nanoparticles for electronic applications. *J. Mater. Sci.* **2009**, *44*, 1076−1081. (b) Preface. In *Sustainable Nanotechnology and the Environment: Advances and Achievements*; Shamim, N., Sharma, V. K., Eds.; *ACS Symposium Series*; American Chemical Society, 2013; Vol. *1124*, p ix. (c) Xie, J.; Lee, J. Y.; Wang, D. I. C.; Ting, Y. P. Identification of Active Biomolecules in the High-Yield Synthesis of Single-Crystalline Gold Nanoplates in Algal Solutions. *Small* **2007**, *3*, 672−682 (accessed Feb 21, 2023).

(11) Zhao, Z.; Sun, J.; Xing, S.; Liu, D.; Zhang, G.; Bai, L.; Jiang, B. Enhanced Raman scattering and photocatalytic activity of TiO2 films with embedded Ag nanoparticles deposited by magnetron sputtering. *J. Alloys Compd.* **2016**, *679*, 88−93.

(12) Gromov, D. G.; Pavlova, L. M.; Savitsky, A. I.; Trifonov, A. Y. Nucleation and growth of Ag nanoparticles on amorphous carbon surface from vapor phase formed by vacuum evaporation. *Appl. Phys. A* **2015**, *118*, 1297−1303.

(13) Jalili, M.; Ghanbari, H.; Moemen Bellah, S.; Malekfar, R. High-quality liquid phase-pulsed laser ablation graphene synthesis by flexible graphite exfoliation. *J. Mater. Sci. Technol.* **2019**, *35*, 292−299.

(14) Zhang, A.; Zhou, J.; Das, P.; Xiao, Y.; Gong, F.; Li, F.; Wang, L.; Zhang, L.; Wang, L.; Cao, Y.; et al. Revisiting Metal Electrodeposition in Porous Anodic Alumina: Toward Tailored Preparation of Metal Nanotube Arrays. *J. Electrochem. Soc.* **2018**, *165*, D129−D134.

(15) Chen, M.; Wang, C.; Wei, X.; Diao, G. Rapid Synthesis of Silver Nanowires and Network Structures under Cuprous Oxide Nanospheres and Application in Surface-Enhanced Raman Scattering. *J. Phys. Chem. C* **2013**, *117*, 13593−13601.

(16) Hsieh, C.-T.; Tzou, D.-Y.; Pan, C.; Chen, W.-Y. Microwave-assisted deposition, scalable coating, and wetting behavior of silver nanowire layers. *Surf. Coat. Technol.* **2012**, *207*, 11−18.

(17) Aziz, N.; Faraz, M.; Pandey, R.; Shakir, M.; Fatma, T.; Varma, A.; Barman, I.; Prasad, R. Facile Algae-Derived Route to Biogenic Silver Nanoparticles: Synthesis, Antibacterial, and Photocatalytic Properties. *Langmuir* **2015**, *31*, 11605−11612.

(18) Vishnevetskii, D. V.; Mekhtiev, A. R.; Perevozova, T. V.; Ivanova, A. I.; Averkin, D. V.; Khizhnyak, S. D.; Pakhomov, P. M. l-Cysteine as a reducing/capping/gel-forming agent for the preparation of silver nanoparticle composites with anticancer properties. *Soft Matter* **2022**, *18*, 3031−3040.

(19) Deshmukh, A. R.; Dikshit, P. K.; Kim, B. S. Green in situ immobilization of gold and silver nanoparticles on bacterial

nanocellulose film using Punica granatum peels extract and their application as reusable catalysts. *Int. J. Biol. Macromol.* **2022**, *205*, 169−177.
(20) Yao, Y.; Cao, S.; Zhang, X.; Yan, J.; Li, W.; Whittaker, A. K.; Zhang, A. Microconfinement from Chitosan Oligosaccharides for Mild Synthesis of Silver Nanoparticles. *ACS Appl. Nano Mater.* **2022**, *5*, 4350−4359.
(21) Tran, M.-T.; Nguyen, L.-P.; Nguyen, D.-T.; Le Cam-Huong, T.; Dang, C.-H.; Chi, T. T. K.; Nguyen, T.-D. A novel approach using plant embryos for green synthesis of silver nanoparticles as antibacterial and catalytic agent. *Res. Chem. Intermed.* **2021**, *47*, 4613−4633.
(22) Taglietti, A.; Diaz Fernandez, Y. A.; Amato, E.; Cucca, L.; Dacarro, G.; Grisoli, P.; Necchi, V.; Pallavicini, P.; Pasotti, L.; Patrini, M. Antibacterial Activity of Glutathione-Coated Silver Nanoparticles against Gram Positive and Gram Negative Bacteria. *Langmuir* **2012**, *28*, 8140−8148.
(23) Piccapietra, F.; Allué, C. G.; Sigg, L.; Behra, R. Intracellular Silver Accumulation in Chlamydomonas reinhardtii upon Exposure to Carbonate Coated Silver Nanoparticles and Silver Nitrate. *Environ. Sci. Technol.* **2012**, *46*, 7390−7397.
(24) Choi, H.; Lee, J.-P.; Ko, S.-J.; Jung, J.-W.; Park, H.; Yoo, S.; Park, O.; Jeong, J.-R.; Park, S.; Kim, J. Y. Multipositional Silica-Coated Silver Nanoparticles for High-Performance Polymer Solar Cells. *Nano Lett.* **2013**, *13*, 2204−2208.
(25) Ye, H.; Chen, J.; Hu, Y.; Li, G.; Fu, X.-Z.; Zhu, P.; Sun, R.; Wong, C.-P. One-pot synthesis of two-dimensional multilayered graphitic carbon nanosheets by low-temperature hydrothermal carbonization using the in situ formed copper as a template and catalyst. *Chem. Commun.* **2020**, *56*, 11645−11648.
(26) (a) Ye, K.; Li, Y.; Yang, H.; Li, M.; Huang, Y.; Zhang, S.; Ji, H. An ultrathin carbon layer activated CeO2 heterojunction nanorods for photocatalytic degradation of organic pollutants. *Appl. Catal., B* **2019**, *259*, 118085. (b) Li, Y.; Xia, Y.; Liu, K.; Ye, K.; Wang, Q.; Zhang, S.; Huang, Y.; Liu, H. Constructing Fe-MOF-Derived Z-Scheme Photocatalysts with Enhanced Charge Transport: Nanointerface and Carbon Sheath Synergistic Effect. *ACS Appl. Mater. Interfaces* **2020**, *12*, 25494−25502. (c) Wang, Y.; Chen, D.; Zhang, J.; Jie Tang Balogun, M.; Wang, P.; Tong, Y.; Huang, Y. Charge Relays via Dual Carbon-Actions on Nanostructured BiVO4 for High Performance Photoelectrochemical Water Splitting. *Adv. Funct. Mater.* **2022**, *32*, 2112738 (accessed June 11, 2023).
(27) (a) Nagamori, M.; Funazukuri, T. Glucose production by hydrolysis of starch under hydrothermal conditions. *J. Chem. Technol. Biotechnol.* **2004**, *79*, 229−233 (accessed June 13, 2023). (b) Möller, M.; Nilges, P.; Harnisch, F.; Schröder, U. Subcritical Water as Reaction Environment: Fundamentals of Hydrothermal Biomass Transformation. *ChemSusChem* **2011**, *4*, 566−579 (accessed June 13, 2023).
(28) Tekin, K.; Karagöz, S.; Bektaş, S. A review of hydrothermal biomass processing. *Renewable Sustainable Energy Rev.* **2014**, *40*, 673−687.
(29) Titirici, M.-M.; Antonietti, M. Chemistry and materials options of sustainable carbon materials made by hydrothermal carbonization. *Chem. Soc. Rev.* **2010**, *39*, 103−116.

https://doi.org/10.1021/acsomega.3c01554
ACS Omega 2023, 8, 23607−23612